Received: 30 March 2022 | Revised: 28 November 2022 | Accepted: 3 December 2022

DOI: 10.1111/pce.14511

ORIGINAL ARTICLE

Plant, Cell & Environment WILEY

Three-dimensional analysis of membrane structures associated with tomato spotted wilt virus infection

Jiansheng Guo[1,2] | Guan Wang[2] | Li Xie[3] | Xinqiu Wang[3] | Lingchong Feng[2] | Wangbiao Guo[2] | Xiaorong Tao[4] | Bruno M. Humbel[2,5] | Zhongkai Zhang[6] | Jian Hong[3]

[1]Department of Pathology of Sir Run Run Shaw Hospital, Zhejiang University School of Medicine, Hangzhou, China

[2]Center of Cryo-Electron Microscopy, Zhejiang University School of Medicine, Hangzhou, China

[3]Center of Analysis and Measurement, Zhejiang University, Hangzhou, China

[4]Department of Plant Pathology, Nanjing Agricultural University, Nanjing, China

[5]Imaging, Okinawa Institute of Science and Technology (OIST), Okinawa, Japan

[6]Yunnan Provincial Key Laboratory of Agri-Biotechnology, Institute of Biotechnology and Genetic Resources, Yunnan Academy of Agricultural Sciences, Kunming, China

Correspondence

Bruno M. Humbel, Center of Cryo-Electron Microscopy, Zhejiang University School of Medicine, 310058 Hangzhou, China.
Email: Bruno.Humbel@oist.jp

Zhongkai Zhang, Yunnan Provincial Key Laboratory of Agri-Biotechnology, Institute of Biotechnology and Genetic Resources, Yunnan Academy of Agricultural Sciences, 650223 Kunming, China.
Email: zhongkai99@sina.com

Jian Hong, Center of Analysis and Measurement, Zhejiang University, 310029 Hangzhou, China.
Email: jhong@zju.edu.cn

Funding information

National Natural Science Foundation of China; Natural Science Foundation of Zhejiang Province

Abstract

To study viral infection, the direct structural visualization of the viral life cycle consisting of virus attachment, entry, replication, assembly and transport is essential. Although conventional electron microscopy (EM) has been extremely helpful in the investigation of virus–host cell interactions, three-dimensional (3D) EM not only provides important information at the nanometer resolution, but can also create 3D maps of large volumes, even entire virus-infected cells. Here, we determined the ultrastructural details of tomato spotted wilt virus (TSWV)-infected plant cells using focused ion beam scanning EM (FIB-SEM). The viral morphogenesis and dynamic transformation of paired parallel membranes (PPMs) were analyzed. The endoplasmic reticulum (ER) membrane network consisting of tubules and sheets was related to viral intracellular trafficking and virion storage. Abundant lipid-like bodies, clustering mitochondria, cell membrane tubules, and myelin-like bodies were likely associated with viral infection. Additionally, connecting structures between neighboring cells were found only in infected plant tissues and showed the characteristics of tubular structure. These novel connections that formed continuously in the cell wall or were wrapped by the cell membranes of neighboring cells appeared frequently in the large-scale 3D model, suggesting additional strategies for viral trafficking that were difficult to distinguish using conventional EM.

KEYWORDS

3D reconstruction in large volume, focused ion beam scanning electron microscopy, viral morphogenesis, viral trafficking

1 | INTRODUCTION

Virus infection induces extensive membrane and organelle rearrangements that may be involved in processes such as viral morphogenesis, intracellular trafficking and intercellular transport (de Castro Martin et al., 2017; Kozieł et al., 2018; Laliberté & Sanfaçon, 2010; Snijder et al., 2020; Weisberg et al., 2017). Benefiting from the development of novel techniques, including immuno-electron microscopy (EM), fluorescent protein fusion, and confocal microscopy, an avenue of investigation at the interface of molecular virology and cell biology has emerged. As with previous studies based on novel techniques, the visualization of viral components and host cells with a greater three-dimensional (3D) volume at the nanoscale contributes to obtaining more structural information about extensive membrane and organelle rearrangements in infected cells. Through 3D analysis of the membrane structures associated with plant virus infection, a pore in the external membrane of Melon necrotic spot virus that altered mitochondria connecting the lumen of the dilation with the cytoplasm (Gómez-Aix et al., 2015), endoplasmic reticulum (ER)-derived membrane spherules that were the sites for Beet black scorch virus replication (Cao et al., 2015), and remodeled chloroplast membranes in Barley stripe mosaic virus-infected cells (Jin et al., 2018) were identified and their functions were confirmed based on their structural information and molecular mechanism.

Tomato spotted wilt virus (TSWV) is a typical member of the *Tospovirus* genus within the family *Bunyaviridae* and is ranked second among the top 10 most economically important viruses worldwide (Scholthof et al., 2011; Walker et al., 2021). As the most well-studied *Tospovirus*, TSWV consists of enveloped, spherical particles containing a tripartite RNA genome (Griffiths & Rottier, 1992; Pettersson, 1991). The molecular biology of TSWV infection has been studied using various model plants and animal systems (Feng et al., 2013, 2016; Kikkert et al., 2001; Leastro et al., 2017; Lewandowski & Adkins, 2005; Paape et al., 2006; Ribeiro et al., 2008). TSWV replication, transcription, and particle assembly take place in the cytoplasm (Francki & Grivell, 1970; Ie, 1971; Kikkert et al., 1999; Zhang et al., 2016). In previous studies based on two-dimensional (2D) EM images and immunolocalization analysis, nucleocapsid aggregates and the paired parallel membranes (PPMs) were thought to be involved in TSWV replication, while double-enveloped particles (DEVs) and single-enveloped particles (SEVs) were distinguished and clustered within ER membranes. Several possible models for the morphogenesis of tospovirus particles, including morphogenesis at the intracellular membranes of the ER or the Golgi system, have been presented (Kikkert et al., 1999; Kitajima et al., 1992).

Although these previous analyses of the morphogenesis of TSWV have provided informative glimpses of cell ultrastructure and viral interactions, the 3D structural information of whole cells at a large volume have remained lacking. In the present study, experiments were conducted to re-examine the ultrastructural features of TSWV-infected plant cells by focused ion beam scanning EM (FIB-SEM), allowing for the analysis of the viral morphogenesis, intracellular trafficking, and intercellular transport at the nanoscale resolution with a large 3D volume (Peddie et al., 2022). Combining computer image processing with FIB-SEM, a large amount of comprehensive 3D information on cell substructures was obtained and novel ultrastructures related to viral infection were established.

2 | MATERIALS AND METHODS

2.1 | Plant materials and virus inoculation

Nicotiana benthamiana was systemically virally infected with TSWV. TSWV was propagated and maintained in *Nicotiana rustica*. Virus-infected plants were grown in a glasshouse maintained at 22°C with a 16 h light/8 h dark cycle.

2.2 | Samples preparation

Samples of systemically infected *N. rustica* leaves were taken for EM analysis. All leaf samples were collected 5–11 days after inoculation with TSWV and fixed quickly for 24 h in 2.5% glutaraldehyde (TED PELLA, Lot No.: 2171002) with 0.1 M phosphate buffer (pH 7.4). The tissue blocks were then washed in phosphate buffer and treated with a solution containing equal volumes of 2% OsO_4 (TED PELLA, Lot No: 4008-160501) and 3% potassium ferrocyanide (Sigma, CAS: 14459-95-1) in phosphate buffer (0.1 M) for 1 h on ice. After rinsing with double-distilled water (ddH_2O), the samples were incubated in 1% thiocarbohydrazide (Sigma, CAS: 2231-57-4) (in water) for 20 min at room temperature. Then, the samples were washed in double-distilled water (ddH_2O) and treated with 2% aqueous OsO_4 for 30 min at room temperature. After rinsing with ddH_2O, the samples were immersed in 1% aqueous uranyl acetate overnight at 4°C. The samples were then washed in ddH_2O and incubated in 0.66% lead nitrate (Sigma, CAS: 10099-74-8) diluted in 0.03 M L-aspartic acid (Sigma, CAS: 56-84-8) (pH 5.5) for 30 min at 60°C, and then dehydrated and flat-embedded in EPON 812 resin (EMS, cat. no: 14900) for 48 h at 60°C.

2.3 | Data collection

Resin blocks that contained leaf tissue were carefully trimmed using a trimmer (EM TXP; Leica) until the resin around the tissue was removed and leaf tissue in the resin block face could be observed. The resin blocks were then mounted on a 90° stub and coated with platinum by an ion sputtering apparatus (EM ACE200; Leica) for 300 s. To obtain the target area, a scanning electron microscope (Teneo VS; Thermo Fisher) with an ultramicrotome in its specimen chamber was used, which enabled the synchronous trimming of the resin blocks and acquisition of the electron microscopic image of the sample. After identifying the target area, the resin blocks were transferred to a 45° pre-tilted SEM stub and then coated with platinum by ion sputtering apparatus (EM ACE200; Leica) for 300 s.

Imaging was performed using a dual beam SEM (FIB Helios G3 UC; Thermo Fisher). The data were collected in the serial surface view mode with a slice thickness of 5 nm at 30 kV and 0.79 nA. Each serial surface was then imaged with 2 kV acceleration voltage and 0.2 nA current in backscatter electron mode with an in-column backscatter electron detector (ICD). The tilt angle of the sample stage was 7° while the milling was carried out. When pictures were taken by electron beam, the tilt angle was changed to 45°. The image frame size was set to 4096 × 3536 pixels with a dwell time of 5 µs per pixel. To study the process of viral assembly and trafficking, including the morphology of PPMs (Sample 1), dissociative DEVs and PPMs (Sample 2), mature virus accumulated in the ER (Sample 3), the ER membrane network and the unusual channel across one cell connecting another two cells (Sample 4), the long channel between the cell membrane and the cell wall (Sample 5), the plasmodesmata and channel-like structure in the cell wall (Sample 6), ultra-large volume structure of uninfected N. benthamiana cells (Sample 7) and the 3D ultrastructure of uninfected plant cells (Sample 8), the image resolution of each sample was different to obtain more structural details or a larger horizontal field width. The section thickness and pixel size for each sample are listed in Supporting Information: Table S1.

2.4 | Image processing and segmentation

The images were aligned, filtered, manually segmented, and used to generate surfaces in Amira 6.8 (Thermo Fisher Scientific).

2.5 | 3D reconstruction and presentation

The surfaces generated in Amira were exported as MRC files. Chimera was used to reassemble the structures, and the segmentation artifacts were carefully removed. The resulting Chimera projects were used in the videos (Supporting Information: Movies 1–16) and static images were exported. The volumes and length of all reconstructed structures were calculated using the label analysis tool in Amira 6.8.

2.6 | Immune EM

Samples (1 × 1 mm) were excised from the leaves of *N. benthamiana* plants infected with TSWV. The sample tissues were fixed in 2% paraformaldehyde (w/v)+0.1% glutaraldehyde (v/v), dehydrated in graded ethanol at 4°C, and embedded in K4M resin (Cat. # 14340, EMS) at −25°C. Ultrathin sections (100 nm) were mounted on formvar-coated grids with a ultramicrotome (EM UC7, Leica). For immunogold labeling, the transmission EM (TEM) sections were incubated in 1% BSA buffer for 10 min, and then for 1 h in 1:200 v/v diluted rabbit polyclonal antibody against TSWV encoded Gc (Kindly granted by Prof. Xiaorong Tao), ADP-ribosylation factor (ARF; Agrisera), and ER retension signal HDEL (a peptide with four amino-acid, his-asp-glu-leu) (Agrisera). The sections were rinsed with PB, and then incubated in 1:30 v/v diluted goat antirabbit IgG conjugated with gold particles for 1 h. After several rinses with PB, the sections were examined with a transmission electron microscope (H7650; Hitachi).

2.7 | Statistical analysis

Manual counting was used to determine the number of tubules in the edges of PPMs in 3D space. The distribution of virus particle was quantified by measuring the volume of 3D data using the Labeling Analysis function in the Amira 6.8 software (Thermo Fisher). Data were statistically analyzed by two-tailed *t* test or one-way analysis of variance using GraphPad Prism (GraphPad Software; La Jolla). $^{*}p < 0.05$; $^{**}p < 0.01$; $^{***}p < 0.001$. Graphs were generated using OriginPro (OriginLab; Northampton) and GraphPad Prism.

3 | RESULTS

3.1 | PPMs are the site of TSWV particle morphogenesis

N. benthamiana were inoculated with TSWV particles and samples were taken between 5 and 11 days after inoculation. A lot of investigations by 2D TEM was carried out and the times of appearance of different structures which have previously been reported to be associated with TSWV maturation (Ie, 1971; Kikkert et al., 1999; Kitajima et al., 1992) were shown in Supporting Information: Table S2. Taking the appearance of all TSWV maturation-associated structures in systemically infected leaf cells 9 days after inoculation into consideration, samples for 3D analysis by FIB-SEM were harvested 9 days after inoculation with TSWV. *N. benthamiana* systemic viral infections with TSWV resulted in rough, yellow leaves, which are typical features of viral infection (Figure 1a). Successful TSWV infection was also verified by an immunogold labeling test, in which the glycoprotein Gc of TSWV was found to accumulate with virus particles (Figure 1b). For large-volume ultrastructural analysis of infected leaf tissues, samples were harvested according to the times of appearance of different structures obtained by 2D TEM and FIB-SEM tomography was employed. In the early stage of infection, some dense material, presumably nucleocapsids, appeared near the newly formed PPMs (Figure 1c). With increasing infection duration, a large amount of the amorphous dense material was detected around curved PPM (Figure 1d). In another area of the infected cell, dense material was found in vesicle-like structures that were associated directly with edges of PPMs (Figure 1e,f). The dense material visible in 2D EM images increased in volume (Figure 1g–i). To confirm that these structures were a transitional form of mature DEVs, further ultrastructural analyses were conducted and a large number of DEVs

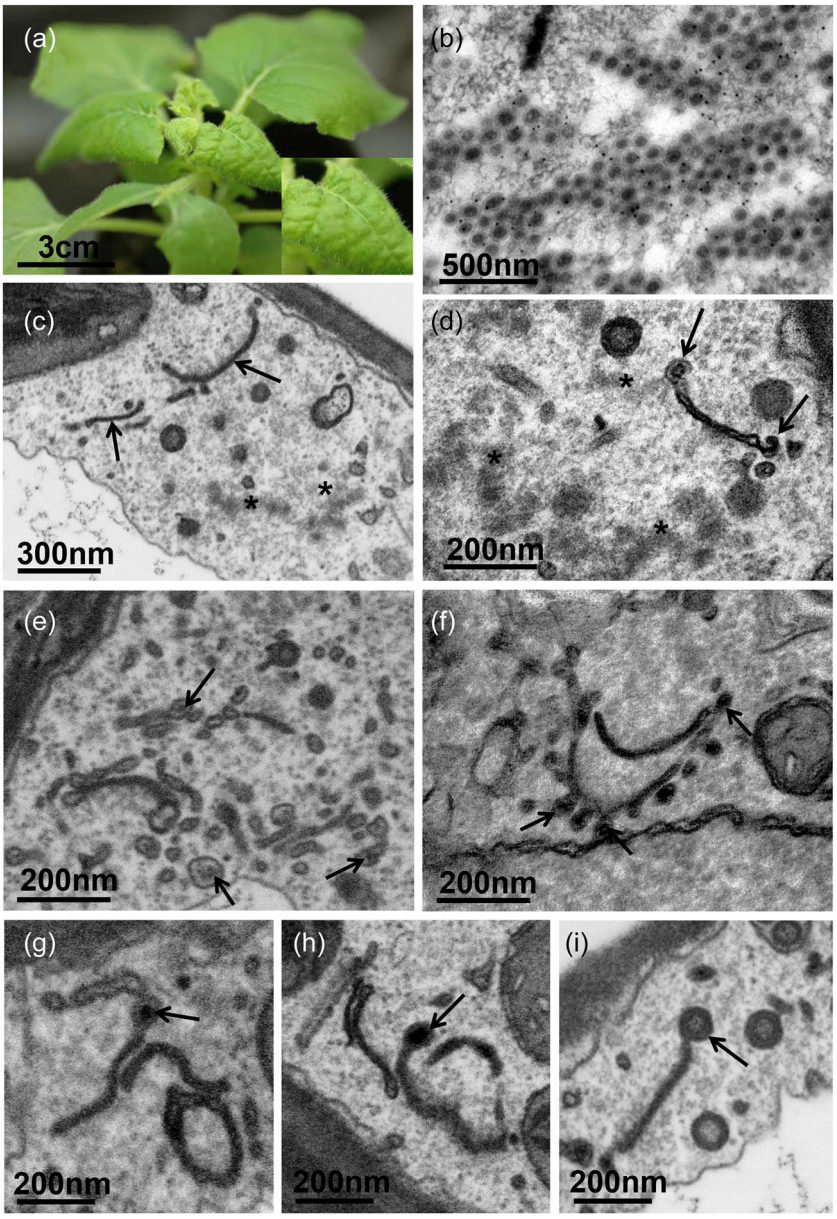

FIGURE 1 Electron micrographs of tomato spotted wilt virus (TSWV)-infected plant cells showing the process of viral assembly. (a) *Nicotiana benthamiana* plants systemically virally infected with TSWV. The infected leaves are partly yellow and rough. (b) Immunogold labeling of glycoprotein Gc in TSWV-infected *N. benthamiana* cells showing many positive signals in the accumulation area of virus particles. (c) A small amount of dense material (*), presumably nucleocapsids, appears near the newly formed paired parallel membranes (PPMs) (indicated by arrows) formed by modification of Golgi stacks. (d) With increasing infection time, a large amount of dense material (*) appears and is close to curved PPMs (indicated by arrows) where dense material is found, indicating that nucleocapsids may be wrapped by PPMs. (e) In the following infection process, vesicle-like structures containing dense material (indicated by arrows), presumably nucleocapsids, are present in nearby PPMs. (f) Vesicle-like structures containing dense material (indicated by arrows) may be directly associated with PPMs. (g)–(i) The dense material (arrows) visible in two-dimensional electron microscopy (EM) images show increases in volume. The double-enveloped particles (DEVs) connect to PPMs directly (i).

were found in the vicinity of PPMs, and one DEV-like dilation on the edge of PPMs suggested that DEVs were formed by the PPMs (Figure 1i).

To investigate the 3D architecture of PPMs and confirm the origin of PPMs, whole PPMs at different stages of infection were reconstructed. Many PPMs with one pie-like structure were identified, and their morphogenesis was studied. The tomographic reconstruction suggested that dense nucleocapsid material in the cytoplasm was wrapped by curving membranes at the edge of PPMs with a diameter of 410.36 ± 17.01 nm (Figure 2a, Supporting Information: Movie 1), and a suitable space was formed for viral assembly (Figure 2b, Supporting Information: Movie 2). Compared with PPMs at the early stage of infection, abundant branched tubules with a diameter of 608.28 ± 21.45 nm that contained dense nucleocapsid material arose from the edges of PPMs at later stages (Figure 2c,d, Supporting Information: Movies 3 and 4, Supporting Information: Figure 1A). This suggested that the formation of branched tubules was related to viral assembly. In some instances, many tubules at the edges of PPMs displayed expanded heads where dense material, presumably nucleocapsids, accumulated (Figure 2e, Supporting Information: Movie 5). A 3D model of a PPM with a semi-transparent membrane showed that nucleocapsids in expanded tubules and DEVs connected frequently with branched tubules (Figure 2e,f, Supporting Information: Figure 1B). Further investigations were conducted, and several PPMs with branched tubules were frequently found to be close to each other (Figure 2g). In some areas, many more PPMs were found close together, and numerous DEVs appeared nearby (Figure 2h). These characteristics were similar to those of Golgi cisternae, which suggests that PPMs may originate from Golgi bodies. This speculation was supported by the positive

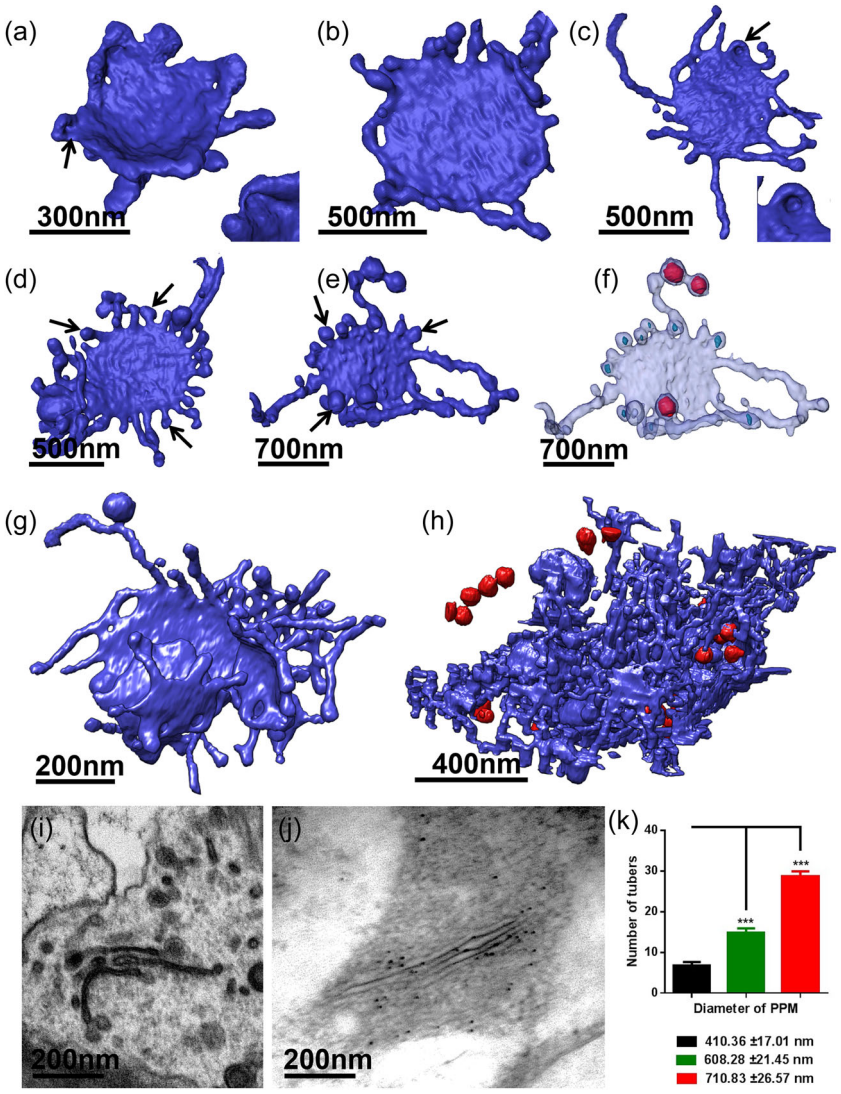

FIGURE 2 Three-dimensional reconstruction of whole paired parallel membranes (PPMs) at different stages showing the three-dimensional (3D) morphology of PPMs and viral assembly. (a) PPM showing a pie-like structure at the early stage of viral infection with ubiquitous caveolae (shown by arrows) where nucleocapsids are wrapped by the membrane. (b) Obvious small tubules appear at the edges of PPMs where nucleocapsids are wrapped. (c) Abundant branched tubules arising from the edges of PPMs suggest that the formation of branched tubules is related to viral assembly. Many tubules at the edges of PPMs display expanded heads (indicated by arrows) where dense material, presumably nucleocapsids, accumulates (d) and (e), as shown in two-dimensional (2D) images (Figure 1c,d). (f) 3D model of PPMs in (e) with semi-transparent membranes (blue) showing the nucleocapsids in expanded tubules (navy) and double-enveloped particles (DEVs; shown in red) connected with branched tubules. (g) Several PPMs with branched tubules are close to each other. (h) Many more PPMs than those shown in (g) were close together, and numerous DEVs appeared nearby. (i) PPM structure showing extended and curved Golgi cisternae with vesicle-like structures containing dense material. (j) Immunogold labeling of PPM structures with antibody against ADP-ribosylation factor (ARF). (k) Statistical analysis of PPM tubules during the increase of PPM diameter (15 PPMs from five to six infected plant cells are shown). [Color figure can be viewed at wileyonlinelibrary.com]

result of immunogold labeling of PPM structures with antibody against ADP-ribosylation factor (ARF), which is located in Golgi bodies (Figure 2i,j). The diameter of the pie-like structures at the late stage of viral infection was 710.83 ± 26.57 nm. The results suggest that the size of PPMs increases during the process of viral assembly. Statistical analysis of PPM tubules during the increase of PPM diameter indicated that viral assembly frequently occurred during the development of PPMs (Figure 2f).

3.2 | Intracellular transport of TSWV

DEVs are single viral particles in the cytoplasm. To reveal more details about DEVs, 2D ultrastructural analysis of infected cells was performed. Numerous DEVs appeared around PPMs (Figure 3a). Imaging at high resolution revealed tail-like structures of DEVs (Figure 3b), which was confirmed by 3D reconstruction (Figure 3c,d). In total, 190 DEVs from 6 regions of different cells all exhibited tail-like structures. This is the first report of these tail-like structures. However, their function remains unknown. One possible function is that this structure may contribute to the transportation of dissociated DEVs to the ER during the following stage of viral infection. This conjecture was strongly supported by the tail targeting the ER membrane (Figure 3e) and different morphological characteristics of ER tubules containing virus particle-like structures (Figure 3f–i). Immunogold labeling of tail-like structures of DEVs with antibody against HDEL, which is located in the ER, indicates that this structure may play a key role in mediating the fusion of DEVs and the ER membrane (Figure 3j). To establish the intercellular transport of TSWV through quantitative analysis, virus particles were divided into several types according to their distribution, including in the cytoplasm (type I), targeting to ER tubules (type II), targeting to ER cisternae (type III), and inside of dilated ER (type IV). Statistical analysis of viral particles in different locations in infected cells suggested that DEVs fused with ER tubules specifically and moved through the ER membrane transport system (Figure 3k).

The ER, consisting of interconnected tubules and sheets, usually displays obvious lumen formed by two membranes where many

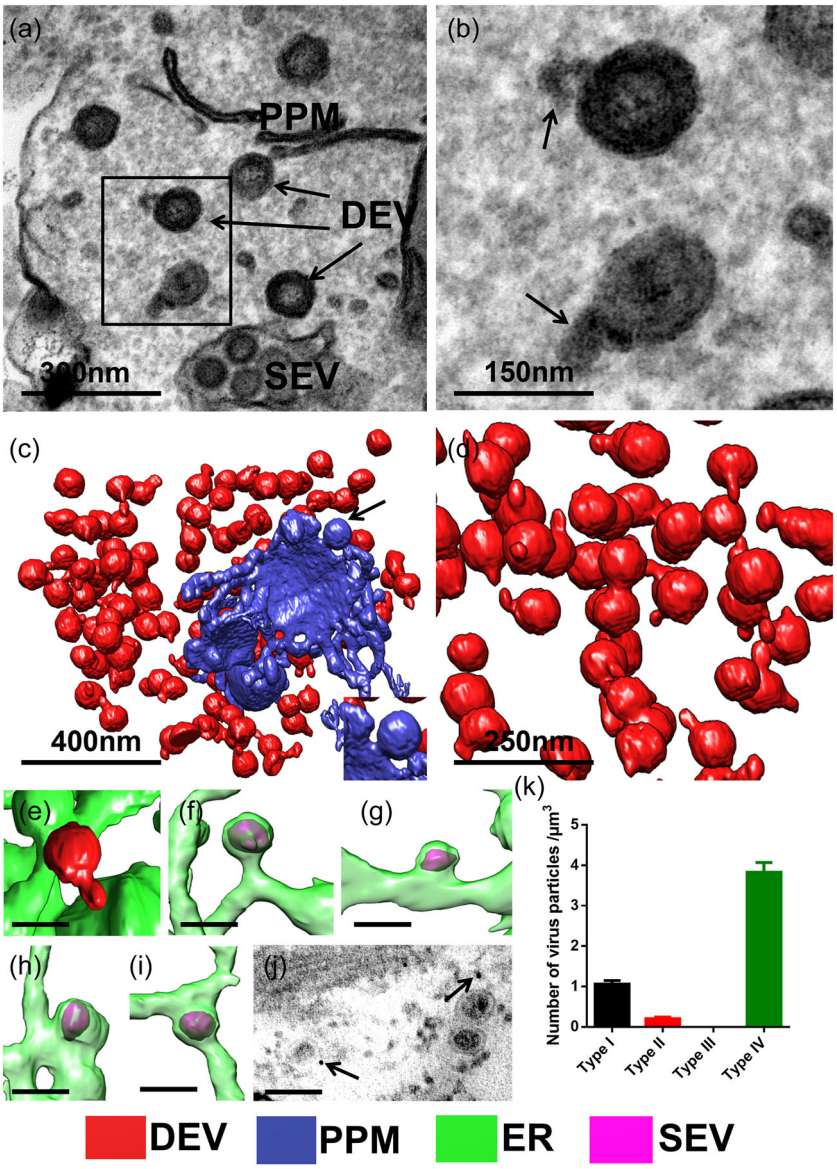

FIGURE 3 Three-dimensional (3D) reconstruction of double-enveloped particles (DEVs) and paired parallel membranes (PPMs). (a) Single two-dimensional (2D) slice showing DEV formation through budding from the PPM. (b) Magnification of the boxed region in (a) showing tail-like structures of DEVs. (c) A 3D reconstruction (a) created by focused ion beam scanning electron microscopy (FIB-SEM) reveals one PPM (blue) surrounded with abundant dissociative DEVs (red) and the budding of newly formed virus particles (indicated by the arrow). (d) Higher magnification of (c) showing distinct DEV tail-like structures. (e) The tail of DEV targeting the endoplasmic reticulum (ER) membrane (green) was close to the ER. (f)–(h) Different morphological characteristics of ER tubules containing virus particles suggest the fusion of tail of DEVs with ER. (i) One virus particle appears in the dilation of ER tubules. (j) Immunogold labeling of DEVs with antibody against HDEL. (k) Statistical analysis of viral particles in different locations of the cell. [Color figure can be viewed at wileyonlinelibrary.com]

ribosomes appear. In 3D space, the ER membrane network resembles a fishing net (Figures 4a and 6a). Compared with the ER, Golgi bodies exhibit more parallel membranes and numerous vesicles around the body. Moreover, Golgi membranes without the ribosome are smooth and often connect to vesicles at the edge. The cellular endomembrane system, including the ER and Golgi bodies, is exploited by viruses to promote multiple steps of the infection cycle. PPM are unique membrane structures that arise from TSWV infection. Usually, PPMs have one smooth membrane body without black particles that is distributed in membranes like the ER. 3D modeling show that PPMs with one pie-like structure displayed abundant branched tubules at their edges, unlike Golgi, which had vesicles connecting to the edge of the membrane body. 3D analysis of infected cells at the late stage of infection indicated that DEVs and the ER membrane fused (Figure 4a, Supporting Information: Movie 7). The 3D architecture of the ER membrane network containing interconnected tubules and sheets (cisternae) revealed aggregated virus particles involved in expanding the ER membrane cisternae and individual DEVs connected with tubules rather than cisternae (Figure 4c,f), which suggested that virus particles might move to a storage location through the ER tubular network. The single-enveloped (particles) SEVs in the intumescent ER membrane (Figure 4b,e) and the fusion of DEV with the ER membrane where agminated virus particles appeared (Figure 4d,g) suggested that SEVs were formed by the fusion of the outer membrane of DEV. Further 3D data on mature virus particles in ER revealed that SEVs could accumulate in the space of the expanding ER in large numbers (Figure 5). Interestingly, individual DEVs around the ER membrane network appeared to wait before entering the ER at random (Figure 5a–c, Supporting Information: Movie 8), which indicated that some virus particles had to move to the storage location through ER tubules. Under some unusual circumstances, a large amount of SEVs filled in almost all space in the ER cisternae (Figure 5d, Supporting Information: Movie 9). The 3D visualization of this area revealed that almost all the space in

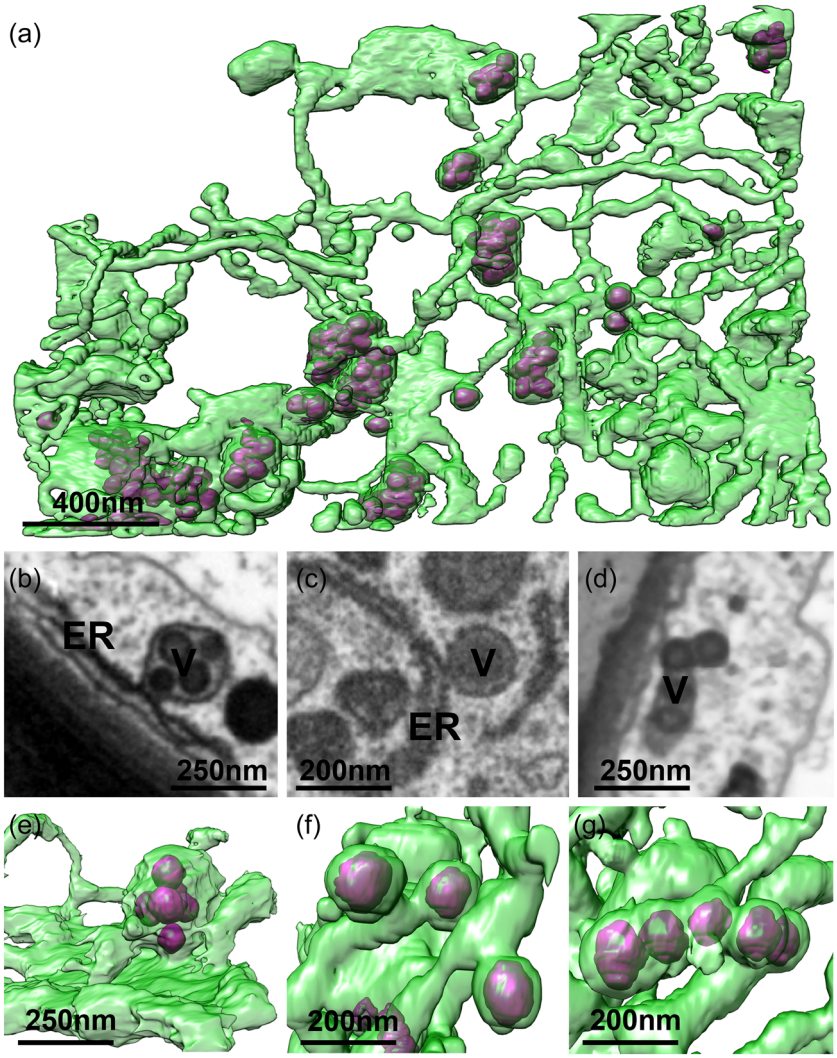

FIGURE 4 Distribution of viral particles in endoplasmic reticulum (ER) tubules and cisternae, showing single particles and agminated particles. (a) Overview of the virus-induced structures, showing part of the ER membrane network (green) containing interconnected tubules and sheets (cisternae), where virus particles (pink) appear. (b) Agminated virus particles accumulate inside of intumescent ER membrane. V, virus. (c) Single virus particles connecting with the ER membrane. (d) DEVs displaying fusion with agminated virus particles in the ER. (e)–(g) Reconstruction of structures in (b)–(d), respectively, by focused ion beam scanning electron microscopy (FIB-SEM), displaying the fusion of DEVs and the ER in different ways. [Color figure can be viewed at wileyonlinelibrary.com]

the ER membrane network was filled with virus particles (Figure 5e). ER tubules that looked like cirrus and were postulated to serve as a platform for the intercellular transport of macromolecules clung to the plasma membrane in parallel (Figure 5e, Supporting Information: Movie 9). Quantitative analysis of dissociated virus particles and virus particles inside inflated ER lumen during infection indicated that newly formed virus particles rapidly entered the ER lumen after being released from PPMs (Figure 5f).

To determine whether organelles were associated with virus infection, the 3D structure of infected cells in ultra-large volumes (7.16×10^3 μm^3) was investigated, and SEVs, DEVs, myelin-like structures (Supporting Information: Figure 1C), lipid-like bodies (Supporting Information: Figure 1D), mitochondria (Supporting Information: Figure 1F), cell membranes, chloroplasts, and the membrane network consisting of PPMs, interconnected ER tubules, and cisternae were analyzed (Figure 6a–c, Supporting Information: Movie 10). Unusually abundant lipid-like bodies close to the membrane network, agminated mitochondria surrounded by the ER (Figure 6d), and numerous cell membrane bulges tightly associated with the ER network (Figure 6b, Supporting Information: Figure 1E) were the most obvious characteristics of infected cells, which indicated the possible role of these organelles in viral replication or intercellular transport. In the present work, lipid-like bodies reported by previous studies (Ie, 1971) displayed obvious membrane structures and close relationships with the ER (Supporting Information: Figure 1D). In contrast, no lipid-like bodies were found in uninfected cells. Considering the phospholipid membrane outside the capsid protein of TSWV, the suggested role of lipid-like bodies may be the source of phospholipid molecules for viral assembly. Myelin-like structures were often found near the area of viral assembly in the collected samples of infected leaf tissues (Figure 6e). The 3D map of infected cells in a large volume displayed the virus factory, including virion assembly, fusion, intracellular transport, and storage.

3.3 | Novel structural features for the intercellular transport of TSWV

Plasmodesma-mediated macromolecular transport plays important roles in plant–pathogen interactions. Plant viruses may use different

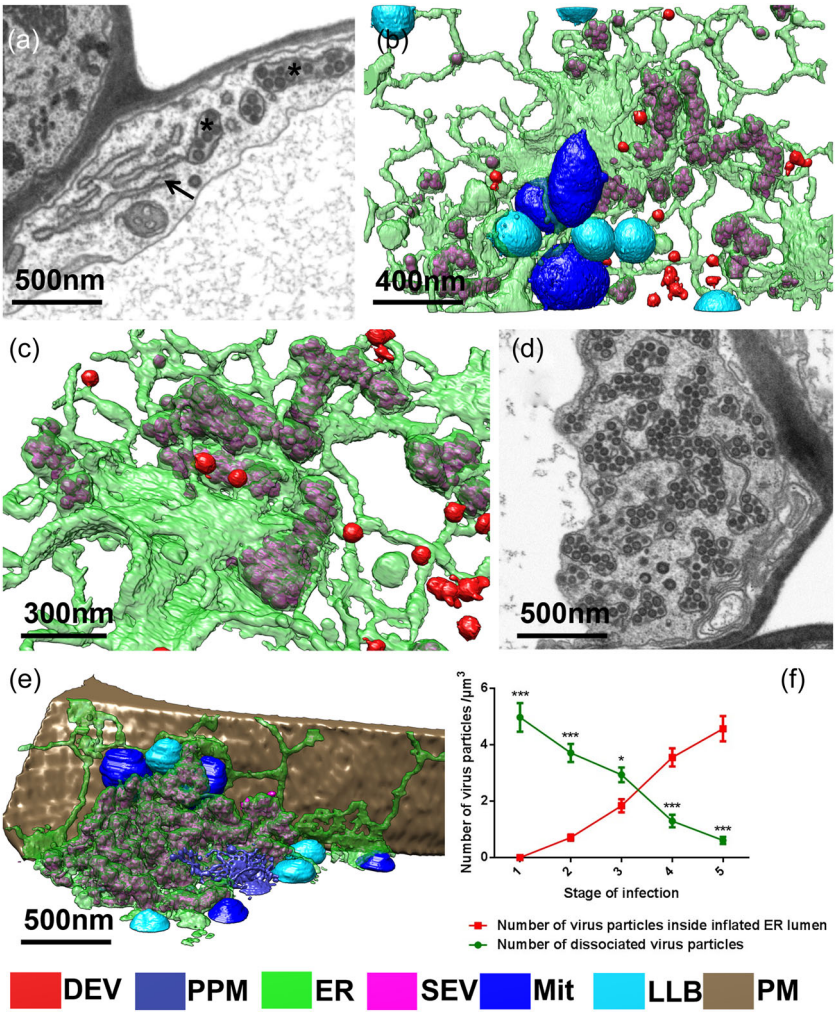

FIGURE 5 Large amounts of mature virus accumulated in the endoplasmic reticulum (ER) cisternae and tubules, which were close to lipid-like bodies, mitochondria, and the plasma membrane. (a) Single slice of three-dimensional (3D) focused ion beam scanning electron microscopy (FIB-SEM) stack from part of an infected cell revealing ER cisternae (indicated by an arrow) and single-enveloped particles (SEVs) (*) in the intumescent ER membrane. (b) Segmentation of structures in (a) indicate the ER membrane network (green) and the location of SEVs (pink), double-enveloped particles (DEVs) (red), mitochondria (blue), and lipid-like bodies (sky blue). (c) Higher magnification of (b) showing DEVs close to the ER tubules. (d) In some areas, larger amounts of SEVs filled in inflated ER cisternae with one extreme way that almost all space in the ER lumen was filled with virus particles. (e) 3D visualization of the ultrastructure in (d) revealing that almost all space in the ER membrane network (green) is filled with virus particles (pink). ER tubules (green) that look like cirrus cling to the plasma membrane (brown) in parallel. Lipid-like bodies (sky blue), mitochondria (blue), and PPM (baby blue) are distributed around the storage location of the virus. (f) Statistical analysis of dissociated virus particles and virus particles inside inflated ER lumen during infection (14–16 cells from 3 experiments). Mit, mitochondria; PM, plasma membrane; LLB, Lipid-like bodies. [Color figure can be viewed at wileyonlinelibrary.com]

host cell transport machineries to move from one cell to another through plasmodesmata. In the present study, some novel structural characteristics associated with the intercellular transport of TSWV were distinguished by FIB-SEM (Figure 7). One stacked and single virus particle was detected in the space formed from the modified cell membrane (Figure 7a,b, Supporting Information: Movie 11). It seemed likely that the virus was released into the intercellular space, similar to exocytosis in mammalian cells. The obtained 3D structure revealed that the ER membrane network contained a large amount of mature virus that closely surrounded the spiky, modified cell membrane (Figure 7c,d, Supporting Information: Movie 11).

To examine the possible mechanisms of viral intercellular movement through the cell wall, the investigation focused on the cell walls of infected cells at the late stage of infection. Inflated and fragmented cell walls with channel-like structures were frequently detected (Figure 7e,f, Supporting Information: Movie 12). The diameters of these channels ranged from 96.61 ± 5.32 nm, and their morphological structures were irregular (Figure 7h). A side view of the 3D model of the cell wall showing the bidirectional expansion of the cell wall is shown in Figure 7g and Supporting Information: Movie 12. The cell membrane was also inflated, and some vesicles were detected in the space formed by the expansion (Figure 7i). The hole that crossed the expanded cell wall and allowed the channel-like structure to pass through was distinguished in the top view of the constructed 3D model (Figure 7j,k). The plasmodesmata and channel-like structure were compared in another 3D model of TSWV-infected plant cells, which confirmed that this channel-like structure was quite different from the plasmodesmata, which displayed a membrane-lined channel tightly encased in the cell wall (Supporting Information: Figure 2, Supporting Information: Movie 13). To further explore the intercellular transport of TSWV, several plant cells were investigated at an ultra-large volume. Serial sections of the same TSWV-infected plant tissue displayed a single long channel that expanded from one cell through the neighboring cell to another cell (Figure 8a–f, Supporting Information: Movie 14). The diameter of this channel was 63.69 ± 3.76 nm. The ER membrane that contained virus appeared to be tightly associated with the end of the channel (Figure 8a). In the 3D model (Supporting Information: Movie 14), the channel-like structure was completely wrapped by the cell membrane of neighboring cells, which indicated that there was no direct connection between the neighboring cells and the channel-like structure (Figure 8g,h). In other words, the novel channel passed over one cell to connect other two cells. Further 3D data (190.33 μm^3) of the infected cells revealed that the long channel

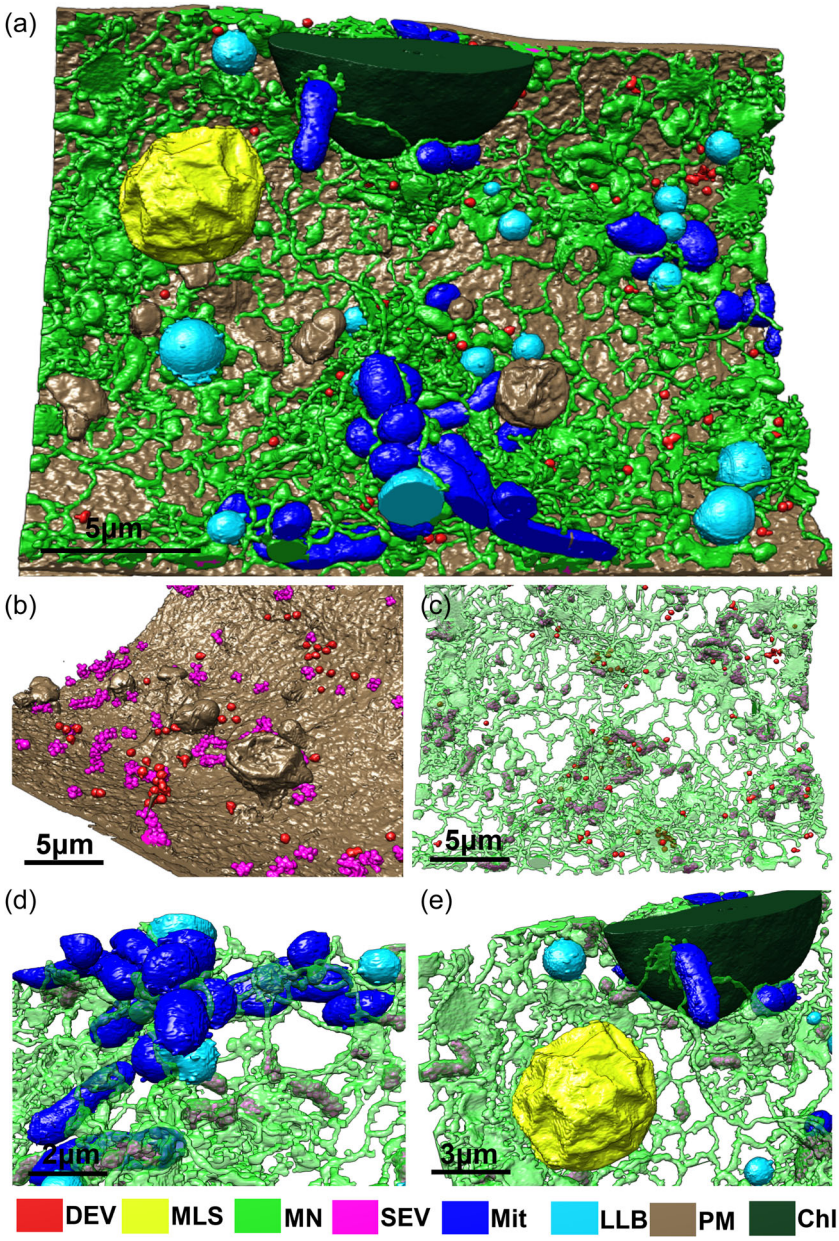

FIGURE 6 Characteristics of infected cells revealed at a large scale by focused ion beam scanning electron microscopy (FIB-SEM). (a) Three-dimensional surface rendering of the spatial relation of single-enveloped particles (SEVs) (pink), double-enveloped particles (DEVs) (red), lipid-like bodies (sky blue), mitochondria (blue), the plasma membrane (brown), myelin-like structures (yellow), chloroplasts (dark green), and the membrane network (green) consisting of paired parallel membranes (PPMs), interconnected endoplasmic reticulum (ER) tubules, and cisternae. Lipid-like bodies and mitochondria accumulated in the area where abundant membrane structures appeared. ER tubules were arranged in parallel on the plasma membrane. (b) Abundant plasma membranes formed from caveolae in the region where a large amount of virus appeared. (c) SEVs accumulated in intumescent ER membranes, and DEVs were randomly distributed near the ER. (d) Lipid-like bodies and mitochondria were closely surrounded by ER tubules. (e) Myelin-like structures visible in (a) were associated with the membrane network. Mit, mitochondria; PM, plasma membrane; LLB, lipid-like bodies; MLS, myelin-like structures; Chl, chloroplast; MN, membrane network. [Color figure can be viewed at wileyonlinelibrary.com]

connecting the endocytic vesicles and inner components of the cell was wrapped by a plasma membrane (Figure 9, Supporting Information: Movie 15). The diameter of this channel was 78.53 ± 4.87 nm. The channel was surrounded by ER tubules containing abundant virus particles (Figure 9a,b). In this area, the inflated ER lumen containing virus particles was found to fuse with the plasma membrane (Figure 9l,m). The long channel structure appeared between the plasma membrane and the cell wall, close to the opening of the ER lumen to the plasma membrane (Figure 9m). After hiding lipid-like bodies, mitochondria, chloroplasts, the inner membrane network, and virus particles by image analysis, it was found that the channel within the cell was wrapped by an invaginated cell membrane, and the channel acted as a bridge to connect neighboring endocytic vesicles (Figure 9c,k). Serial sections of infected cells revealed details of the electron-dense channel structure, curving cell membrane, and endocytic vesicles (Figure 9d–j). This channel was encased by a plasma membrane, similar to that shown in Figure 8. However, a cross section of the long channel structure revealed a single dark spot surrounded by a membrane-like structure (Figure 9n), which was not found in Figure 8. In addition, the abundant endocytic vesicles that were connected in a series by the channel exhibited obviously different characteristics, which indicated that this could be used as a novel endocytic recycling pathway in viral transport.

4 | DISCUSSION

The 3D EM of large volumes allowed for the detection of ultrastructural features of TSWV-infected cells, including PPMs, DEVs, the ER membrane network, and novel channels connecting

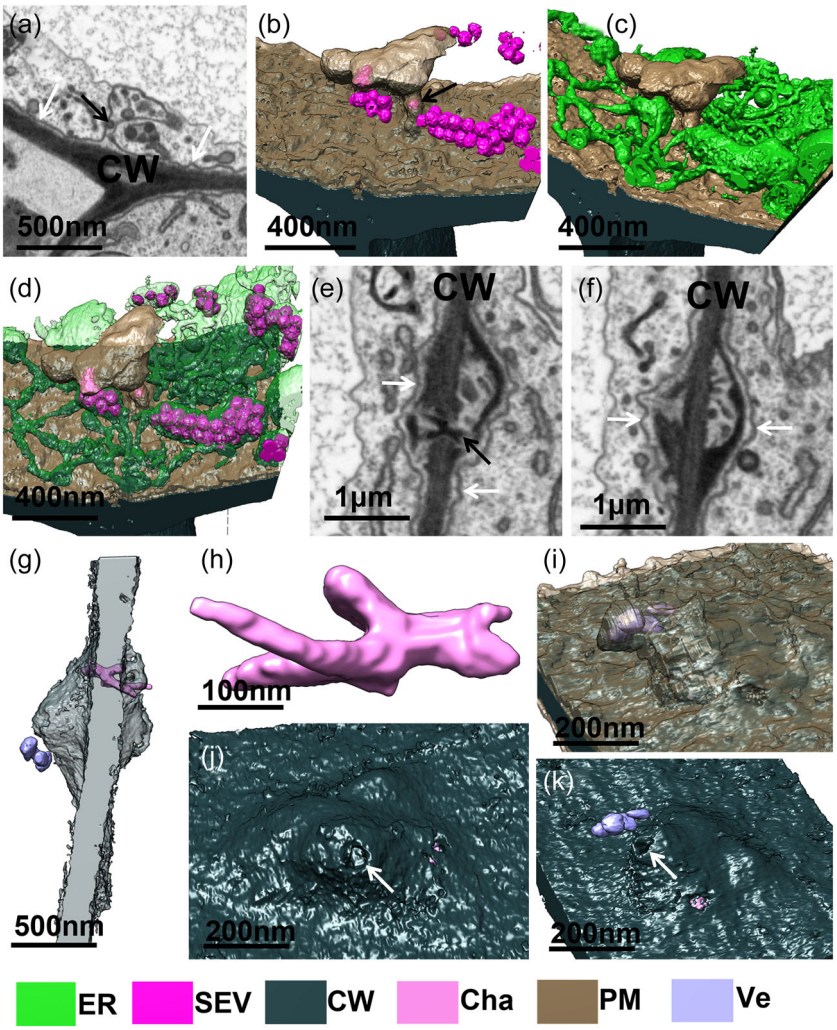

FIGURE 7 Three-dimensional (3D) reconstruction of the raised plasma membrane and cell wall showing viral intercellular transport. (a) One stacked and single virus particle (black arrow) was found in the space formed from the modified plasma membrane (white arrow). CW, cell wall. (b) The 3D reconstruction of focused ion beam scanning electron microscopy (FIB-SEM) data in (a) displayed spiky modified plasma membrane (brown) that contained one virus particle (indicated by an arrow). (c) The spiky structure shown in (b) was closely surrounded by the ER membrane network (green). (d) Numerous virus particles (pink) distributed in pocket-like ER membranes (green). (e), (f) Slice view of two different locations from the FIB-SEM stack showing the channel (black arrow) through the cell wall (e). As the cell wall became inflated and fragmented, the plasma membrane (white arrows) was also inflated (f). (g) Side view of the 3D model showing the bidirectional expansion of the cell wall. (h) The atactic channel (carmine) through the cell wall. (i) A plasma membrane (brown) wrapped the swollen cell wall and vesicles (bluish violet) appeared in the folded membrane space. (j) Top view of cell wall showing the hole (arrow) through the expanding cell wall. (k) View of (j) from another perspective displays vesicles (bluish violet) close to the hole (arrow) formed by the expansion of the cell wall. CW, cell wall; Cha, channel; PM, plasma membrane; Ve, vesicles. [Color figure can be viewed at wileyonlinelibrary.com]

plant cells, and to elucidate the process of viral infection. These findings provide new perspectives on how TSWVs replicate and undergo intracellular/intercellular transport. The results revealed that the ER was primarily subverted by TSWVs to transport virus particles from the cytoplasm to the plasma membrane. The unique budding of DEV from PPMs and the role of DEV tails in fusion with ER membranes suggest that viral morphogenesis and intracellular transport may need reevaluation. These data strongly suggest an alternative model (Figure 10) in which (i) viral assembly occurs in the PPM and the tails of DEVs act as messengers while virions enter the ER lumen; (ii) viral infection induces extensive swelling and tubulation of the ER throughout the cell, from the cytoplasm to the plasma membrane; (iii) virus particles are transported intercellularly through the fusion of the ER with the plasma membrane and the frequently observed fractured cell wall, and viral components pass through the plasmodesmata (Li et al.,2009; Storms et al., 1995; Zhu et al., 2019); and (iv) the long channel structures wrapped by the plasma membrane inside the cell connect endocytic vesicles or neighboring cells, which suggests that the intercellular transport of virus may occur in the long channel structures and endocytic vesicles.

In the present study, single 2D slices revealed the expected views of curving and wrapping PPMs, dense nucleocapsid-like material, DEVs, and SEVs (Kikkert et al., 1999; Zhang et al., 2016). Normally, Golgi shows many parallel membranes and numerous vesicles around the body. The 3D reconstruction of PPMs, especially the newly formed PPMs, had similar characteristics to the 3D architecture of dictyosomes reported in earlier studies (Koga et al., 2017; Wanner et al., 2013), which strongly indicated that PPMs were formed from Golgi. Furthermore, Golgi bodies with abundant saccules and vesicles in uninfected *N. benthamiana* cells exhibited normal ultrastructures (Supporting Information: Figure 3, Supporting Information: Movie 16) that were similar to the parallel membrane of PPM. In addition, the result of immunogold labeling of PPM structures revealed the presence of ARF which is known to be in the Golgi Apparatus. Numerous PPM flocked together appeared like modified Golgi stacks with cisternae moving away from each other. These results provided more evidence that PPM originated from Golgi. In the 3D model, obvious cavities at the edge of PPMs without branched tubules were found. Dense material, which was assumed to consist of nucleocapsids, frequently appeared close to the curving PPM. These findings indicated that nucleocapsids were enveloped by

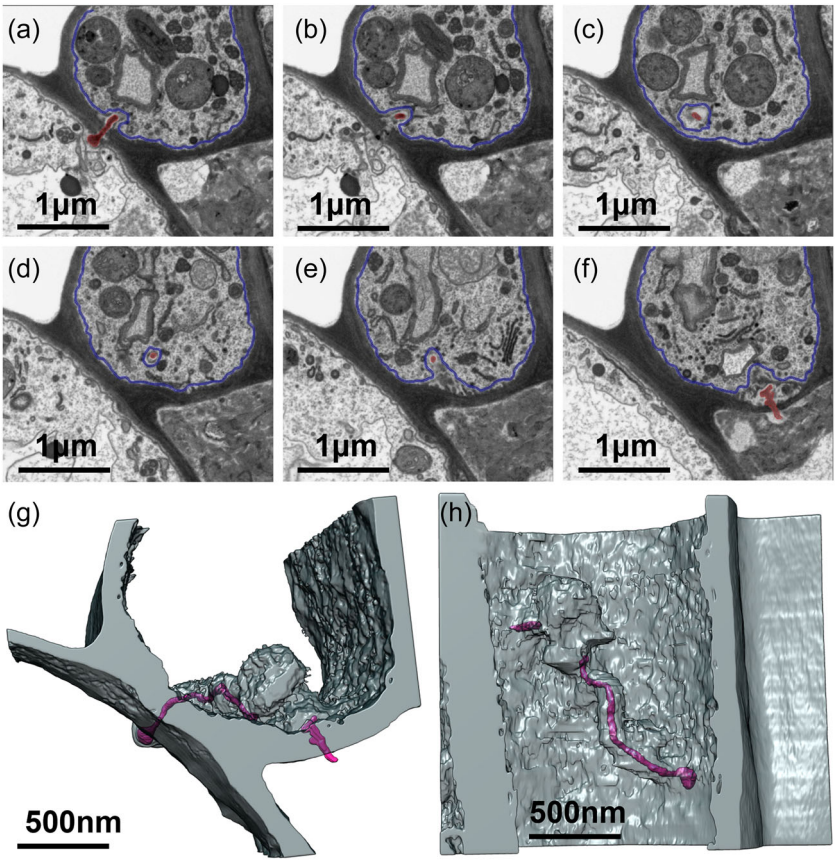

FIGURE 8 Investigation of the three-dimensional (3D) focused ion beam scanning electron microscopy (FIB-SEM) stack showing an unusual channel-like structure crossing one cell to connect another two cells. (a)–(f) Serial sections of *tomato* spotted wilt virus (TSWV)-infected plant tissue showing a long channel (red) expanding from one cell through a neighboring cell to another cell. The channel-like structure is completely wrapped by the plasma membrane (blue) of the neighboring cell. (g) Side view of 3D model showing the channel-like structure (pink) across the cell wall connecting to neighboring cells, as also shown in (a) and (f). (h) Top view of the 3D model showing the channel-like structure (pink) wrapped by the plasma membrane. [Color figure can be viewed at wileyonlinelibrary.com]

the edges of PPMs. The morphogenesis of abundant expanding tubules containing dense material at the edge of the PPM confirmed that viral assembly took place in these nucleocapsid-containing compartments. Additionally, tubular compartments that originated from the edge of the PPM were presented in this study for the first time. The function of these tubules is unknown. It is possible that these tubular compartments contribute to the budding of DEVs from PPMs by reducing the contact area between them. Numerous dissociated DEVs in this investigation showed a tail-like structure that was suggested to be responsible for the fusion with the ER membrane. The absence of this tail-like structure in previous studies may have been due to the suboptimal fixation of the membrane. Furthermore, the small size of the tail made it very easy to miss by conventional 2D TEM imaging. With the benefit of advances in large imaging volume made possible by FIB-SEM, this tail-like structure was revealed and its possible role in viral infection was analyzed.

The fusion of DEVs with each other and with the ER leads to the formation of mature SEVs clustered inside large vesicles within the cytoplasm of plant cells (Kikkert et al., 1999). The 3D reconstruction using Amira software showed that almost the entire ER consisted of tubules and cisternae, SEVs were clustered in the expanding pocket-like ER membrane, and single DEVs seemed to connect with ER tubules to fuse specifically. In some cases, a large amount of SEVs filled in almost all space in the ER cisternae. Based on these investigations, it seems likely that some virus particles need to move to a storage location through ER tubules from the site of fusion. The plant ER is a unique structure that is interconnected among cells via the ER desmotubules in the plasmodesmata across the cell wall, forming a continuous ER network throughout the entire plant (Nakano et al., 2014; Pain et al., 2019; Shen et al., 2014; Stefano et al., 2014). In plant cells, the ER is most probably anchored to the plasma membrane at static points (Sparkes et al., 2009), and it extends into the body of the cell (Griffing, 2010; Sparkes et al., 2011; Ward & Brandizzi, 2004). Structurally, the plasmodesmata are composed of the plasma membrane with a central, modified ER (Maule, 2008). In the present study, interconnected ER tubules and cisternae were determined at the nanoscale in ultra-large volumes, and clustered SEVs appeared in the ER network, whose pattern was similar to that of grapes in grapevine. It seems likely that TSWV particles are packaged and sent to the ER network in cells for intracellular transport. In addition, compared with the sparse ER network in uninfected plant cells (Supporting Information: Figure 3, Supporting Information: Movie 16), abundant ER tubules and cisternae in TSWV-infected plant cells strongly suggested that the virus could stimulate the host cell to develop an endomembrane system for virus reproduction.

Endocytosis in plants has been described as an endocytic recycling pathway for virus movement and protein transport (Haupt et al., 2005; Lewis & Lazarowitz, 2010; Uchiyama et al., 2014). Large intracellular vesicles attached to the plasma membrane are thought to be responsible for viral cell-to-cell transport. Taking the abundant cell membranes in the cytoplasm at the virus accumulation area into

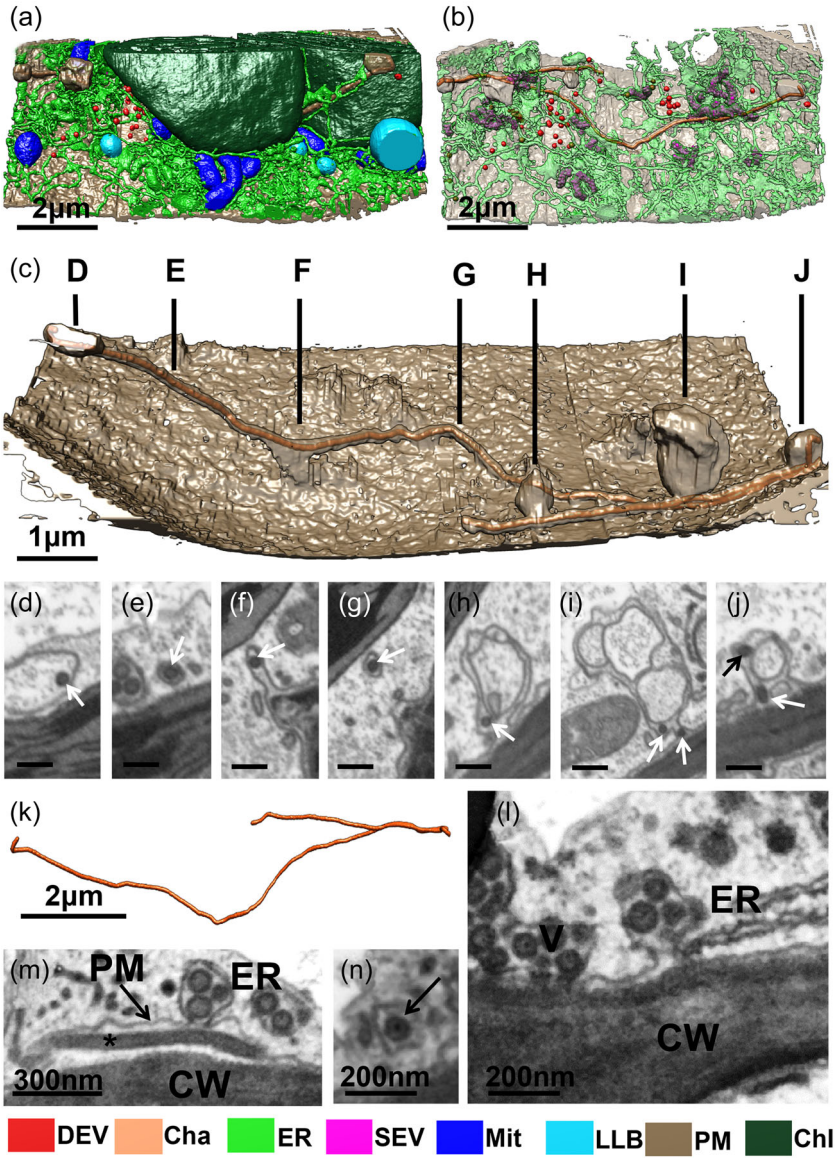

FIGURE 9 Long channel between the cell membrane and cell wall connects the endocytic vesicles and the inner components of the cell. (a) Three-dimensional (3D) reconstruction of a part of a cell at a large volume, showing the spatial relationships between single-enveloped particles (SEVs) (pink), double-enveloped particles (DEVs) (red), lipid-like bodies (sky blue), mitochondria (blue), the plasma membrane (brown), chloroplasts (dark green), and the inner membrane network (green). (b) After removing lipid-like bodies, mitochondria, and chloroplasts, virions appeared in the transparent ER membrane and the long channel structure within cell was wrapped by the cell membrane. (c) High magnification of the membrane, showing details of the endocytic vesicles and long channel structure. (d–j) Serial sections of an infected cell display an electron-dense channel structure (indicated by arrows), a curving cell membrane, and endocytic vesicles (c). Scale bar = 200 nm. (k) 3D model showing the morphological characteristics of the long channel. (l) Inflated endoplasmic reticulum (ER) lumen containing virus particles fused with the plasma membrane. (m) Long channel structure (*) appeared between the plasma membrane (arrow) and the cell wall. The opening of the ER lumen to the plasma membrane was close to the long channel structure. (n) Cross section of the long channel structure (arrow) showing a single dark spot surrounded by a membrane-like structure. Cha, channel; Chl, chloroplast; LLB, lipid-like bodies; Mit, mitochondria; PM, plasma membrane; [Color figure can be viewed at wileyonlinelibrary.com]

consideration, the findings of the present study are in agreement with previous reports on this hypothesis. To move within and between cells, viruses spread between cells in several forms, including viral replication complexes and the passage of viral particles through the plasmodesmata (Heinlein, 2015; Jackson et al., 2009; Lucas, 2006; Peña & Heinlein, 2012; Tilsner & Oparka, 2012; Tilsner et al., 2013). In the present study, stacked and single virus particles in the space formed from modified cell membranes indicate that TSWV may be transported in the form of virions.

Although plasmodesmata play a very important role in intercellular virus movement (Lucas & Lee, 2004; Lucas et al., 2009; Oparka & Roberts, 2001), the size exclusion limit (SEL) of plasmodesmata provides a physical barrier that must be overcome by a virus to successfully move from cell to cell (P. Harries & Ding, 2011). Virus movement proteins (MP) are thought to be necessary factors regulating the SEL of plasmodesmata (Boyko et al., 2000; Gillespie et al., 2002; Su et al., 2010). Viral proteins other than the classically defined MPs have been found to have movement capabilities (P. A. Harries et al., 2009; Liu et al., 2005). In TSWV-infected plant tissues, it has been speculated that viral components pass through the plasmodesmata during the intercellular movement of TSWV (Feng et al., 2016; Zhao et al., 2016). Even so, there remains much work to be done to gain a clear understanding of the requirements for cell-to-cell movement of the huge diversity of plant viruses. Compared with the plasmodesmata of previous studies, the channel connecting two TSWV-infected cells in the present study exhibits unique 3D architecture and a much larger diameter (96.61 ± 5.32 nm) that may allow the viral components pass across the cell wall. Furthermore, inflated and fragmented cell walls near the channel structure and the obvious lacerated regions in the cell walls that allowed the channel structures to pass through were frequently found. This leads this research group to suggest that this channel may be a novel structure caused by viral infection, although it cannot be concluded whether it is an intermediate form of plasmodesmata. The

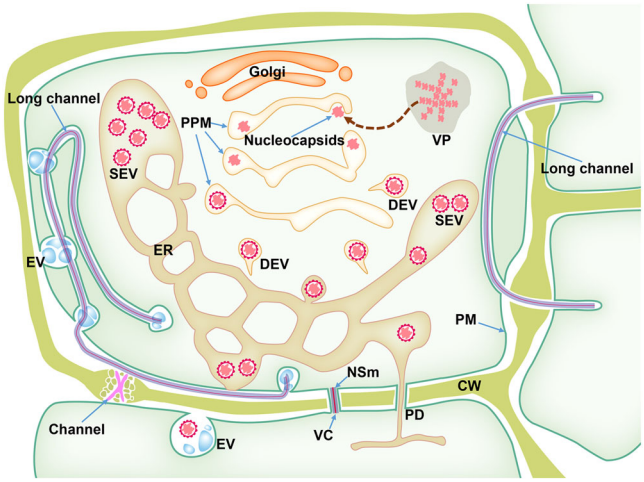

FIGURE 10 Model of the morphogenesis and intracellular and intercellular transport of tomato spotted wilt virus (TSWV) in infected plant cells. Nucleocapsid aggregates (NCA) embedded in viroplasm (VP) appear in cytoplasm and enter Golgi membrane system. Paired parallel membranes (PPMs) are formed from Golgi bodies and exhibit larger diameters during viral assembly. The remodeled tubulo-vesicular endoplasmic reticulum (ER) is unusually abundant in infected plant cells. The nucleocapsids in the cytoplasm are wrapped by the edge of the PPM and transferred to vesicles connected to the PPM by long tubules. TSWV virions appear at the end of tubules and break away to form double-enveloped particles (DEVs) containing a single membranous tail. When virus particles enter the ER lumen at random, the tails contact the ER, accompanied by membrane fusion, and allow virions to enter the ER lumen to form single-enveloped particles (SEVs). Virus particles then move to a storage location along the ER membrane network. The ER containing virus particles fuse with the plasma membrane (PM), forming one opening that allows virus particles to enter the space between the PM and cell wall for intercellular transport. The frequently observed fractured cell wall (CW) may be the channel (pink) allowing virus particles pass through, and the virions are captured by the endocytic vesicles of adjacent cells. Additionally, the abundant endocytic vesicles (EV) connected in series by long channels exhibited obviously different characteristics, suggesting that this may represent a novel endocytic recycling pathway in viral transport. The viral components (VC) may be transported through the long channel from the inside of the cell to the space between the plasma membrane and cell wall, and received by the endocytic vesicles of another cell. In previous studies, it is reported that the movement protein NSm forms a tubule structure within the plasmodesmata (PD) to guide the transport of the viral components into neighboring healthy cells (Zhu et al., 2019). [Color figure can be viewed at wileyonlinelibrary.com]

frequent channel structure with inflated and fragmented cell walls in TSWV-infected cells disappeared in uninfected plant tissues (Supporting Information: Figure 3, Supporting Information: Movie 16), which indicated that the novel channel was closely involved with virus infection.

Another novel connecting-type structure revealed by 3D model at an ultra-large volume was the long channel that expanded from one cell through a neighboring cell and to a third cell. In previous studies, it was reported that the MP NSm of tomato spotted wilt tospovirus could induce tubular structures protruding from the cell surface in systemically infected *N. rustica* mesophyll tissue and insect cells (Storms et al., 1995) and *N. rustica* protoplasts (Goldbach et al., 1997). Specifically, the tubular structures appeared in the plasmodesmata, suggesting their involvement in cell-to-cell movement of the virus during systemic infection (Zhu et al., 2019). In our study, the long unusual channel-like structure was similar with these tubular structures, which suggested that the channel-like structure may come from the inducing of NSm. Moreover, the channel-like structure was completely wrapped by the cell membrane of the neighboring cell, indicating that there was no direct connection between the neighboring cell and the channel-like structure. In other words, the novel and infrequent channel by passed one cell to connect two other cells. It seemed likely that the viral components could be sent directly across one whole cell at a much greater distance, which improved the transport efficiency and stability. Another channel-like structure wrapped by the cell membrane was found between the cell membrane and cell wall, connecting neighboring endocytic vesicles and the inner components of the cell. Taking the close connection between this channel and the ER membrane containing virus particles into consideration, this finding suggests the existence of one novel endocytic recycling pathway in viral transport. In this model, the inner components of cells could be transported in enclosed space to endocytic vesicles, and the transportation could be more selective. Neither of these two types of connecting structures were found in uninfected *N. benthamiana* cells by ultra-large volume analysis (Supporting Information: Figure 4), which suggested that the rearrangement of membranes was related to virus infection and very likely involved with viral transmembrane transports.

In conclusion, large-volume 3D analysis at the nanoscale provided new insights into the ultrastructure of infected plant cells, revealing a large amount of novel morphological information on viral replication, intracellular transport, and intercellular transport (Figure 10). In particular, PPM originating from Golgi is the site of the occurrence of the virus and the tails of DEVs act as messengers while virions enter the ER lumen. Viral infection induces extensive swelling and tubulation of the ER, and intracellular transport of virus particles happens in ER membrane network. Virus particles are transported intercellularly through the fusion of the ER with the plasma membrane and the frequently observed fractured cell wall. The frequently observed channel architecture crossing the cell wall and endocytic vesicles indicated different strategies of viral material transformation from the existing model, such as plasmodesmata. One key biological principle is that structure determines function; the present study revealed detailed information about structure as a foundation for the future elucidation of function.

ACKNOWLEDGMENTS

We thank the Center of Cryo-Electron Microscopy (CCEM) at Zhejiang University for FIB-SEM data collection and 3D reconstruction. This work was supported by grants from the National Natural Science Foundation of China (U1802235) and the Natural Science Foundation of Zhejiang Province (LQ20C040003).

DATA AVAILABILITY STATEMENT

Data available on request from the authors. The data that support the findings of this study are available from the corresponding author upon reasonable request.

REFERENCES

Boyko, V., Ferralli, J., Ashby, J., Schellenbaum, P. & Heinlein, M. (2000) Function of microtubules in intercellular transport of plant virus RNA. *Nature Cell Biology*, 2, 826–832.

Cao, X., Jin, X., Zhang, X., Li, Y., Wang, C., Wang, X. et al. (2015) Morphogenesis of endoplasmic reticulum membrane-invaginated vesicles during Beet Black Scorch Virus infection: Role of auxiliary replication protein and new implications of three-dimensional architecture. *Journal of Virology*, 89, 6184–6195.

de Castro Martin, I.F., Fournier, G., Sachse, M., Pizarro-Cerda, J., Risco, C. & Naffakh, N. (2017) Influenza virus genome reaches the plasma membrane via a modified endoplasmic reticulum and Rab11-dependent vesicles. *Nature Communications*, 8, 1396.

Feng, Z., Chen, X., Bao, Y., Dong, J., Zhang, Z. & Tao, X. (2013) Nucleocapsid of tomato spotted wilt tospovirus forms mobile particles that traffic on an actin/endoplasmic reticulum network driven by myosin XI-K. *The New Phytologist*, 200, 1212–1224.

Feng, Z., Xue, F., Xu, M., Chen, X., Zhao, W., Garcia-Murria, M.J. et al. (2016) The ER-Membrane transport system is critical for intercellular trafficking of the NSm movement protein and tomato spotted wilt tospovirus. *PLoS Pathogens*, 12, e1005443.

Francki, R.I.B. & Grivell, C.J. (1970) An electron microscope study of the distribution of tomato spotted wilt virus in systemically infected *Datura stramonium* leaves. *Virology*, 42, 969–978.

Gillespie, T., Boevink, P., Haupt, S., Roberts, A.G., Toth, R., Valentine, T. et al. (2002) Functional analysis of a DNA-shuffled movement protein reveals that microtubules are dispensable for the cell-to-cell movement of tobacco mosaic virus. *The Plant Cell*, 14, 1207–1222.

Goldbach, R., Bloksma, H., Kormelink, R., van Poelwijk, F., Kassies, W., Kikkert, M. et al. (1997) A protoplast system for studying tomato spotted wilt virus infection. *Journal of General Virology*, 78, 1755–1763.

Gómez-Aix, C., García-García, M., Aranda, M.A. & Sánchez-Pina, M.A. (2015) Melon necrotic spot virus replication occurs in association with altered mitochondria. *Molecular plant-microbe interactions: MPMI*, 28, 387–397.

Griffing, L.R. (2010) Networking in the endoplasmic reticulum. *Biochemical Society Transactions*, 38, 747–753.

Griffiths, G. & Rottier, P. (1992) Cell biology of viruses that assemble along the biosynthetic pathway. *Seminars in Cell Biology*, 3, 367–381.

Harries, P. & Ding, B. (2011) Cellular factors in plant virus movement: at the leading edge of macromolecular trafficking in plants. *Virology*, 411, 237–243.

Harries, P.A., Palanichelvam, K., Yu, W., Schoelz, J.E. & Nelson, R.S. (2009) The cauliflower mosaic virus protein P6 forms motile inclusions that traffic along actin microfilaments and stabilize microtubules. *Plant Physiology*, 149, 1005–1016.

Haupt, S., Cowan, G.H., Ziegler, A., Roberts, A.G., Oparka, K.J. & Torrance, L. (2005) Two plant-viral movement proteins traffic in the endocytic recycling pathway. *The Plant Cell*, 17, 164–181.

Heinlein, M. (2015) Plasmodesmata: channels for viruses on the move. *Methods in Molecular Biology*, 1217, 25–52.

Ie, T.S. (1971) Electron microscopy of developmental stages of tomato spotted wilt virus in plant cells. *Virology*, 43, 468–479.

Jackson, A.O., Lim, H.S., Bragg, J., Ganesan, U. & Lee, M.Y. (2009) Hordeivirus replication, movement, and pathogenesis. *Annual Review of Phytopathology*, 47, 385–422.

Jin, X., Jiang, Z., Zhang, K., Wang, P., Cao, X., Yue, N. et al. (2018) Three-dimensional analysis of chloroplast structures associated with virus infection. *Plant Physiology*, 176, 282–294.

Kikkert, M., Van Lent, J., Storms, M., Bodegom, P., Kormelink, R. & Goldbach, R. (1999) Tomato spotted wilt virus particle morphogenesis in plant cells. *Journal of Virology*, 73, 2288–2297.

Kikkert, M., Verschoor, A., Kormelink, R., Rottier, P. & Goldbach, R. (2001) Tomato spotted wilt virus glycoproteins exhibit trafficking and localization signals that are functional in mammalian cells. *Journal of Virology*, 75, 1004–1012.

Kitajima, E.W., Resende, R.D., de Avila, A.C., Goldbach, R.W. & Peters, D. (1992) Immuno-electron microscopical detection of tomato spotted wilt virus and its nucleocapsids in crude plant extracts. *Journal of Virological Methods*, 38, 313–322.

Koga, D., Ushiki, T. & Watanabe, T. (2017) Novel scanning electron microscopy methods for analyzing the 3D structure of the Golgi apparatus. *Anatomical Science International*, 92, 37–49.

Kozieł, E., Otulak-Kozieł, K. & Bujarski, J. (2018) Ultrastructural analysis of prune dwarf virus intercellular transport and pathogenesis. *International Journal of Molecular Sciences*, 19, 2570.

Laliberté, J.F. & Sanfaçon, H. (2010) Cellular remodeling during plant virus infection. *Annual Review of Phytopathology*, 48, 69–91.

Leastro, M.O., De Oliveira, A.S., Pallás, V., Sánchez-Navarro, J.A., Kormelink, R. & Resende, R.O. (2017) The NSm proteins of phylogenetically related tospoviruses trigger Sw-5b-mediated resistance dissociated of their cell-to-cell movement function. *Virus Research*, 240, 25–34.

Lewandowski, D.J. & Adkins, S. (2005) The tubule-forming NSm protein from tomato spotted wilt virus complements cell-to-cell and long-distance movement of tobacco mosaic virus hybrids. *Virology*, 342, 26–37.

Lewis, J.D. & Lazarowitz, S.G. (2010) Arabidopsis synaptotagmin SYTA regulates endocytosis and virus movement protein cell-to-cell transport. *Proceedings of the National Academy of Sciences*, 107, 2491–2496.

Li, W., Lewandowski, D.J., Hilf, M.E. & Adkins, S. (2009) Identification of domains of the tomato spotted wilt virus NSm protein involved in tubule formation, movement and symptomatology. *Virology*, 390, 110–21.

Liu, J.Z., Blancaflor, E.B. & Nelson, R.S. (2005) The tobacco mosaic virus 126-kilodalton protein, a constituent of the virus replication complex, alone or within the complex aligns with and traffics along microfilaments. *Plant Physiology*, 138, 1853–1865.

Lucas, W.J. (2006) Plant viral movement proteins: agents for cell-to-cell trafficking of viral genomes. *Virology*, 344, 169–184.

Lucas, W.J., Ham, B.K. & Kim, J.Y. (2009) Plasmodesmata - bridging the gap between neighboring plant cells. *Trends in Cell Biology*, 19, 495–503.

Lucas, W.J. & Lee, J.Y. (2004) Plasmodesmata as a supracellular control network in plants. *Nature Reviews Molecular Cell Biology*, 5, 712–726.

Maule, A.J. (2008) Plasmodesmata: Structure, function and biogenesis. *Current Opinion in Plant Biology*, 11, 680–686.

Nakano, R.T., Yamada, K., Bednarek, P., Nishimura, M. & Hara-Nishimura, I. (2014) ER bodies in plants of the Brassicales order: Biogenesis and association with innate immunity. *Frontiers in Plant Science*, 5, 73.

Oparka, K.J. & Roberts, A.G. (2001) Plasmodesmata. A not so open-and-shut case. *Plant Physiology*, 125, 123–126.

Paape, M., Solovyev, A.G., Erokhina, T.N., Minina, E.A., Schepetilnikov, M.V., Lesemann, D.E. et al. (2006) At-4/1, an interactor of the tomato spotted wilt virus movement protein, belongs to a new family of plant proteins capable of directed intra and intercellular trafficking. *Molecular Plant-Microbe Interactions®*, 19, 874–883.

Pain, C., Kriechbaumer, V., Kittelmann, M., Hawes, C. & Fricker, M. (2019) Quantitative analysis of plant ER architecture and dynamics. *Nature Communications*, 10, 984.

Peddie, C.J., Genoud, C., Kreshuk, A. et al. (2022) Volume electron microscopy. *Nat Rev Methods Primers*, 2, 51.

Peña, E.J. & Heinlein, M. (2012) RNA transport during TMV cell-to-cell movement. *Frontiers in Plant Science*, 3, 193.

Pettersson, R.F. (1991) Protein localization and virus assembly at intracellular membranes. *Current Topics in Microbiology and Immunology*, 170, 67–106.

Ribeiro, D., Foresti, O., Denecke, J., Wellink, J., Goldbach, R. & Kormelink, R.J.M. (2008) Tomato spotted wilt virus glycoproteins induce the formation of endoplasmic reticulum- and Golgi-derived pleomorphic membrane structures in plant cells. *Journal of General Virology*, 89, 1811–1818.

Scholthof, K.B.G., Adkins, S., Czosnek, H., Palukaitis, P., Jacquot, E., Hohn, T. et al. (2011) Top 10 plant viruses in molecular plant pathology. *Molecular Plant Pathology*, 12, 938–954.

Shen, Y., Zhao, X., Yao, M., Li, C., Miriam, K., Zhang, X. et al. (2014) A versatile complementation assay for cell-to-cell and long distance movements by cucumber mosaic virus based agro-infiltration. *Virus Research*, 190, 25–33.

Snijder, E.J., Limpens, R.W.A.L., de Wilde, A.H., de Jong, A.W.M., Zevenhoven-Dobbe, J.C., Maier, H.J. et al. (2020) A unifying structural and functional model of the coronavirus replication organelle: Tracking down RNA synthesis. *PLoS Biology*, 18, e3000715.

Sparkes, I., Hawes, C. & Frigerio, L. (2011) FrontiERs: movers and shapers of the higher plant cortical endoplasmic reticulum. *Current Opinion in Plant Biology*, 14, 658–665.

Sparkes, I., Runions, J., Hawes, C. & Griffing, L. (2009) Movement and remodeling of the endoplasmic reticulum in nondividing cells of tobacco leaves. *The Plant Cell*, 21, 3937–3949.

Stefano, G., Hawes, C. & Brandizzi, F. (2014) ER—The key to the highway. *Current Opinion in Plant Biology*, 22, 30–38.

Storms, M.M., Kormelink, R., Peters, D., Van Lent, J.W. & Goldbach, R.W. (1995) The nonstructural NSm protein of tomato spotted wilt virus induces tubular structures in plant and insect cells. *Virology*, 214(2), 485–493.

Su, S., Liu, Z., Chen, C., Zhang, Y., Wang, X., Zhu, L. et al. (2010) Cucumber mosaic virus movement protein severs actin filaments to increase the plasmodesmal size exclusion limit in tobacco. *The Plant Cell*, 22, 1373–1387.

Tilsner, J., Linnik, O., Louveaux, M., Roberts, I.M., Chapman, S.N. & Oparka, K.J. (2013) Replication and trafficking of a plant virus are coupled at the entrances of plasmodesmata. *Journal of Cell Biology*, 201, 981–995.

Tilsner, J. & Oparka, K.J. (2012) Missing links?—The connection between replication and movement of plant RNA viruses. *Current Opinion in Virology*, 2, 705–711.

Uchiyama, A., Shimada-Beltran, H., Levy, A., Zheng, J.Y., Javia, P.A. & Lazarowitz, S.G. (2014) The arabidopsis synaptotagmin SYTA regulates the cell-to-cell movement of diverse plant viruses. *Frontiers in Plant Science*, 5, 584.

Walker, P.J., Siddell, S.G., Lefkowitz, E.J., Mushegian, A.R., Adriaenssens, E.M., Alfenas-Zerbini, P. et al. (2021) Changes to virus taxonomy and to the international code of virus classification and nomenclature ratified by the international committee on taxonomy of viruses. *Archives of Virology*, 166, 2633–2648.

Wanner, G., Schäfer, T. & Lütz-Meindl, U. (2013) 3-D analysis of dictyosomes and multivesicular bodies in the Green alga *Micrasterias denticulata* by FIB/SEM tomography. *Journal of Structural Biology*, 184, 203–211.

Ward, T.H. & Brandizzi, F. (2004) Dynamics of proteins in Golgi membranes: comparisons between mammalian and plant cells highlighted by photobleaching techniques. *Cellular and molecular life sciences: CMLS*, 61, 172–185.

Weisberg, A.S., Maruri-Avidal, L, Bisht, H., Hansen, B.T., Schwartz, C.L., Fischer, E.R. et al. (2017) Enigmatic origin of the poxvirus membrane from the endoplasmic reticulum shown by 3D imaging of vaccinia virus assembly mutants. *Proceedings of the National Academy of Sciences of the United States of America*, 114, 11001.

Zhang, Z., Zheng, K., Dong, J., Fang, Q., Hong, J. & Wang, X. (2016) Clustering and cellular distribution characteristics of virus particles of tomato spotted wilt virus and tomato zonate spot virus in different plant hosts. *Virology Journal*, 13, 11.

Zhao, W., Jiang, L., Feng, Z., Chen, X., Huang, Y. & Xue, F. et al. (2016) Plasmodesmata targeting and intercellular trafficking of tomato spotted wilt tospovirus movement protein NSm is independent of its function in HR induction. *The Journal of General Virology*, 97, 1990–1997.

Zhu, M., van Grinsven, I.L., Kormelink, R. & Tao, X. (2019) Paving the way to tospovirus infection: multilined interplays with plant innate immunity. *Annual Review of Phytopathology*, 57, 41–62.

SUPPORTING INFORMATION

Additional supporting information can be found online in the Supporting Information section at the end of this article.

How to cite this article: Guo, J., Wang, G., Xie, L., Wang, X., Feng, L., Guo, W., et al. (2023) Three-dimensional analysis of membrane structures associated with tomato spotted wilt virus infection. *Plant, Cell & Environment*, 46, 650–664. https://doi.org/10.1111/pce.14511